# Highly Localized Electron Cyclotron Heating and Current Drive with Improved Core Transport in DIII–D

R. Prater,[1] M. Austin,[2] S. Bernabei,[3] K.H. Burrell,[1] R.W. Callis, [1] W.P. Cary,[1]
J.S. deGrassie,[1] C. Fuchs,[4] C.M. Greenfield,[1] Y. Gorelov,[1] R.W. Harvey,[5] J.C. Hosea,[3]
A. Isayama,[6] J. Jayakumar,[7] R.J. La Haye,[1] L.L. Lao,[1] R.A. Legg,[1] Y.-R. Lin-Liu,[1] J. Lohr,[1]
T.C. Luce,[1] M. Makowksi,[7] C.C. Petty,[1] R.I. Pinsker,[1] D. Ponce,[1] S. Pronko,[1]
S. Raftopoulos,[3] E.J. Strait,[1] and K.-L. Wong[3]

[1]General Atomics, P.O. Box 85608, San Diego, California 92186-5608, USA
email: prater@fusion.gat.com
[2]University of Texas, Austin, Texas 78712, USA
[3]Princeton Plasma Physics Laboratory, Princeton, New Jersey 08543 USA
[4]Max Planck Institute für Plasmaphysik, Garching, Federal Republic of Germany
[5]CompX, Del Mar, California, USA
[6]Japan Atomic Energy Research Institute, Naka-machi, Naka-gun, Ibaraki-ken, Japan
[7]Lawrence Livermore National Laboratory, Livermore, California 94550, USA

**Abstract**. Electron cyclotron heating (ECH) and current drive (ECCD) are widely recognized as methods of depositing highly localized power and current in a plasma, based on calculations of wave absorption. The experiments reported here demonstrate through direct analysis of the poloidal field pitch angles measured by the motional Stark effect diagnostic that ECCD can be as localized as theory predicts. This very narrow profile of driven current has been verified even for ELMing H–mode discharges, and observation of full stabilization of neoclassical tearing modes tends to corroborate the calculations of ECCD far off axis even in plasmas with large MHD activity present. The electron heating by EC waves can have dramatic effects on the plasma, creating high central electron temperatures even with very modest ECH power and generating a strong transport barrier in the electron fluid in discharges with strongly reversed central magnetic shear. The electron diffusivity is much smaller than ion neoclassical diffusivity in the narrow barrier which develops just outside the heating location.

## 1. Introduction

Electron Cyclotron Current Drive (ECCD) has been recognized as an effective means of driving plasma current in a localized and controlled way in tokamak configurations, based on theoretical calculations and supported by recent experiments [1,2]. Due to these characteristics, ECCD is useful in many applications in tokamaks. For example, off-axis ECCD is useful in sustaining profiles of plasma current which support improved confinement and stability as in the Advanced Tokamak (AT) program [3], one of the few recognized approaches to steady-state operation of a tokamak. Alternatively, highly localized ECCD can stabilize neoclassical tearing modes [4,5], which constitute an important limitation on tokamak performance. In order to take advantage of these opportunities, it is critical that a detailed comparison of theory and experiment be carried out in order to fully establish the predictive modeling capability needed to optimally apply ECCD. Such a comparison is also useful in identifying physics issues which need to be addressed in the model.

## 2. ECH System

The experiments were carried out on the DIII–D tokamak. The mission of the DIII–D program is to establish the scientific basis for the optimization of the tokamak approach to fusion energy production. In order to further that objective, a high power electron cyclotron heating (ECH) system [6] is being implemented in the DIII–D program in stages. This ECH system operates at a frequency of 110 GHz, which corresponds to the second harmonic of the electron cyclotron frequency at 1.96 T. The high frequency power is generated by gyrotron oscillators, which have been placed in operation as the gyrotron systems become available. Up to three gyrotrons, operating at a power of typically 0.6 MW incident on the plasma each, were used in the experiments presented here. The system is being upgraded to six gyrotrons.

The transmission system carries the ECH power from the gyrotron to the tokamak, a distance of about 80 m, in corrugated waveguide carrying the $HE_{11}$ mode. The waveguide is evacuated to a pressure below $1\times10^{-3}$ Torr, and no vacuum barrier window is present at the tokamak end. This waveguide system has operated flawlessly at an average power density of 90 kW/cm$^2$, with almost no need for power conditioning and no known arcs or other failures. The bends in the transmission line are carried out using miter bends, two of which use sinusoidal corrugated reflecting surfaces to transform the nearly linear polarization of the gyrotron output into the wave polarization at the plasma surface which is calculated to excite exclusively the X–mode.

The wave launching structures employ a waveguide radiator of diameter 6 cm followed immediately by a focussing mirror which reflects the wave onto a steerable mirror. The steerable mirror controls the angles of launch of the wave into the plasma. Two of the antennas, constructed by PPPL and used in most of the work presented here, have a mechanical system which allows both the poloidal and toroidal angles to be changed between discharges. The beam angular divergence in the far-field region is 1.7° (full width at half maximum power), making the beam diameter containing 98% of the power typically 12 cm at the resonance.

The wave polarization was validated before the experiments were carried out. Any wave polarization incident at the plasma edge can be decomposed into a combination of the two normal modes of the plasma, the X–mode and the O–mode. The X–mode is strongly absorbed at the second harmonic for the conditions of the experiment, but the O–mode has wave absorption typically in the range 10%–30%. This makes the O–mode fraction useless for driving net current since wave power absorbed on the two sides of the resonance drives currents in opposite toroidal directions. In order to ascertain that the X–mode is primarily being excited, modulated ECH power was applied at launch angles for which the ray trajectory for the first pass through the plasma was off-axis and for the second pass was near the plasma center [7]. Then the X–mode fraction is fully absorbed at the off-axis location and the O-mode fraction is weakly absorbed there but more strongly absorbed near the center where the opacity is higher since the temperature and density are higher. The relative power in the two modes can be estimated through phase-sensitive detection at the modulation frequency of the profile of temperature fluctuations measured by electron cyclotron emission [7]. By using this measurement technique and systematically varying the wave parameters of inclination and ellipticity so as to follow contours of constant calculated fractional X–mode power, the behavior of the polarizers was shown to correspond well with theory so that the required polarization could be generated with confidence.

A key diagnostic for the determination of the driven current is the motional Stark effect (MSE) system, which measures the pitch angle of the magnetic field lines through polarimetry of emitted radiation from energetic neutrals from a neutral beam injector [8]. The fixed locations of the MSE channels are shown in Fig. 1, along with the ECE channels. The locations of the ECE channels shift in major radius when the toroidal field is changed.

## 3. Localization of Off-axis ECCD

Experiments on off-axis ECCD [1,2] have been analyzed previously using the evolution of the internal magnetic flux [9]. This technique showed that off-axis currents were being driven at the locations predicted by theory, but that the profile of driven current was typically wider than expected. Work by Petty et al. [10] using a simulation approach has shown that the narrowness of the driven current profile determined in this manner is limited by the equilibrium reconstruction, which is unable to fully resolve radial features as narrow as the calculated ECCD profile. This shortcoming is being addressed by increasing the grid size in the reconstruction from 65×65 to 257×257 and by changes in the basis functions which are used to fit $P'$ and $FF'$ in the EFIT equilibrium reconstruction code [11].

Recently we have sought evidence of localized ECCD directly in the MSE data [10]. This view holds that the magnetic field pitch angles measured by MSE are the fundamental

measurements which determine the driven current, so the physical limit on the resolution is that of the MSE channels. Simulations of the evolution of the equilibrium with and without ECCD are used to generate simulated MSE signals. These simulated signals can be compared with experiment, and by finding the best fit of the location, width, and magnitude of the driven current, the profile of ECCD most consistent with the most sensitive diagnostic (MSE) can be determined. Typically, the profiles so determined are narrower than those found from the evolution of the internal magnetic flux, bringing theory and experiment into closer agreement.

The pitch angles measured by MSE can be converted into local measurements of toroidal current through application of Ampere's law, which can be written in cylindrical coordinates as

$$\frac{\partial B_R}{\partial z} - \frac{\partial B_z}{\partial R} = \mu_0 j_\phi \qquad (1)$$

where R is the major radius, z is the vertical position, and $\phi$ is the toroidal angle, and neglecting the displacement current. $B_z$ is found by multiplying the pitch angle by the local toroidal field. Then the quantity $dB_z/dR$ comes directly from the channel-to-channel differences in $B_z$ and R, and $j_\phi$ is proportional to this quantity.

The effect of ECCD can be determined by comparing $dB_z/dR$ determined in this way for two discharges, one with ECCD and one without. The measured change in $dB_z/dR$ during ECCD is not used directly in the current drive analysis, but rather it is compared to a simulation of the change in $dB_z/dR$ since modifications of the Ohmic, bootstrap, and neutral beam currents can also cause a local change in $j_\phi$, and because the quantity $dB_R/dz$ in Eq. (1) cannot be directly measured. The simulation permits these factors to be included self-consistently. A comparison between simulations and experiment is shown in Fig. 2, as well as the calculated profile of ECCD for this discharge. Figure 2(a) shows that nearly all of the ECCD takes place between a single pair of MSE channels near $\rho$=0.3, in excellent agreement with the calculation by the TORAY-GA code and with the simulation shown in Fig. 2(b). The full width of the driven current is about 0.1 in $\rho$.

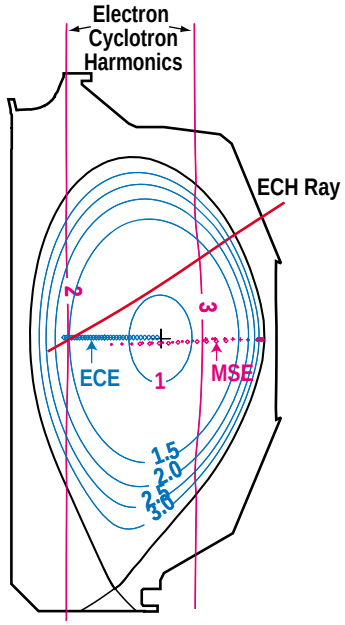


*FIG. 1. (a) Cross-section of the DIII–D plasma, showing the projection of an ECH ray. Also shown are the ECE channels and the MSE channels and some low-order rational surfaces.*

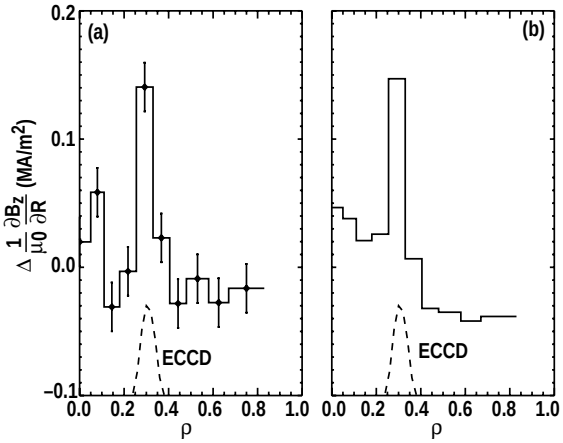


*FIG. 2. Change in the channel-to-channel differences in the MSE signals for (a) experiment and (b) simulation of the same discharge. The dashed curves are the ECCD calculated by the TORAY-GA code for the experimental conditions, not to scale. $I_p$=0.9 MA, $B_T$=1.8 T, $n$=1.8×10$^{19}$ m$^{-3}$, $P_{nbi}$=2.6 MW, $P_{ec}$=0.9 MW.*

The magnitude of driven current can be determined by finding the best fit, in a statistical sense, of the simulated data to the experimental data using the magnitude as a free parameter in the simulation. This process produces a clear minimum in $\chi^2$ for an ECCD of 39±4 kA for

the case of Fig. 2, in agreement with the current drive calculated by the CQL3D Fokker-Plank code [12] of 37 kA.

The driven current determined in this way as a function of minor radius is in good agreement with theory. This is shown in Fig. 3 for a vertical scan of the minor radius from $\rho$=0.1 to $\rho$=0.4. In this figure the vertical axis is the driven current normalized in a natural way [1] by the density and temperature, which change with $\rho$, and the power. The measured points are in agreement with the efficiency calculated by the Fokker-Planck code, except for the outermost point at $\rho$=0.45. For this point the effect is small and the experiment should be repeated at higher power for better resolution. It should be noted that the decrease in efficiency with $\rho$ includes the effects of trapping and also the effect of changes in $n_{||}$ due to modification of the geometry when the ECH launch angles are changed.

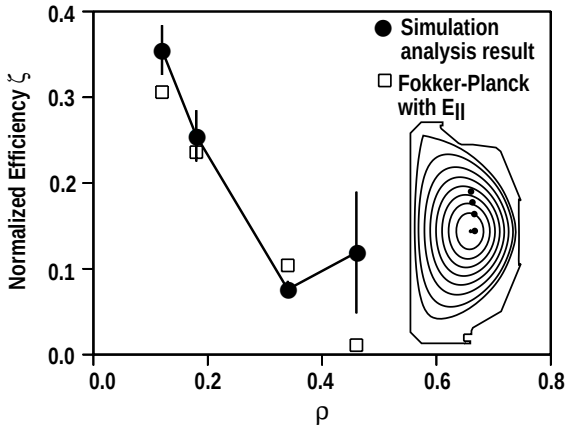


*FIG. 3. Dimensionless ECCD efficiency as a function of normalized minor radius, for a vertical scan of interaction location.The filled circles are results of analysis of the experiment, and the squares are Fokker-Planck calculations including the effects of $E_{||}$.*

Recent experiments are the first to test off-axis ECCD in H–mode plasmas. H–modes are characterized by a higher density and larger density gradient at the edge than L–mode plasmas. The larger density means that the driven current will be smaller, making detection more difficult. Serious issues have also been raised about the effect of the edge gradient on wave refraction and whether the large effect of ELMs on the edge density will scatter the ECH rays and spoil the optics. In order to address these issues, a series of orthogonal scans of $\rho$, magnetic well depth, and $n_{||}$ were carried out. For example, using the PPPL launcher with adjustable poloidal and toroidal angles, it was possible to vary $\rho$ in both the midplane and in a vertical plane, keeping $n_{||}$ constant at 0.4.

These scans require further analysis before details will be available; however, it is possible to see the result of the ECCD directly on the MSE signals as in Fig. 2, even in H–mode. A complicating factor in the analysis is that the radial electric field, $E_r$, contributes significantly to the change in the MSE signals in H–mode. The effects of $E_r$ can be separated from the Bz effects by comparing the changes in MSE channels on the inboard side with those on the outboard side, since $E_r$ has the opposite sign in the two locations. This means that direct analysis of ECCD in H–modes may be limited to $\rho$ less than 0.3, where inboard data are available (Fig. 1).

## 4. Suppression of Neoclassical Tearing Modes to Validate ECCD

Validation of ECCD under conditions typical of high performance discharges is very challenging. Typical AT scenarios have MHD activity present, like ELMs, possibly low level tearing modes, and possibly sawteeth, all of which could affect the efficiency and profile of ECCD. In order to validate ECCD under these conditions, it was necessary to use indirect means to estimate the magnitude, location, and width of the driven current profile. An experiment on suppression of neoclassical tearing modes (NTMs) by localized ECCD provided such an opportunity.

Theory indicates that the neoclassical tearing mode, which grows due to the helical magnetic perturbation caused by the reduction of bootstrap current within the magnetic island forming the tearing mode [13], can be stabilized by driving current within the island by other means, i.e. by ECCD, to compensate for the “missing” bootstrap current [4], or by driving current sufficiently close to the rational surface to flatten the equilibrium current gradient there [14]. Experiments have been performed on the ASDEX-U tokamak [5,15] and the JT-60U

tokamak [16] which confirm that co-ECCD is effective at stabilizing NTMs when the location of the current drive is sufficiently near the rational surface containing the tearing mode.

Experiments on DIII–D have shown full suppression of a m=3/n=2 neoclassical tearing mode by continuous localized ECCD, leading to increased plasma performance. In this case ECCD was applied by aiming the power from two gyrotrons in the co-ECCD direction near the q=3/2 surface. The ECH power was directed to intersect the resonance near the inboard midplane in order to minimize the effect of trapping as shown in Fig. 1. The low $B_T$ causes the third harmonic resonance to enter the plasma, but the absorbed power there is estimated to be less than 20%.The toroidal component of the ECH beam was set to be rather small ($n_{||}$=0.3) in order to maximize the peak of the current density by reducing the Doppler broadening rather than to maximize the total driven current by increasing the Doppler shift. Figure 4 shows traces for a case of complete suppression.

Several of the expected features of NTM stabilization can be seen in Fig. 4. When the ECCD is applied, the amplitude of the island, as characterized by the n=2 Mirnov amplitude, begins decreasing immediately. The time scale of the decrease is hundreds of ms, corresponding to the time scale of inductive effects. When the amplitude reaches 4 G, the rate of decrease becomes much larger and the amplitude of the mode falls to the level of the noise in the measurement as full stabilization of the NTM takes place. Presumably, amplitudes smaller than 4 G correspond to the region of negative growth rate [4]. Even in the presence of subsequent sawteeth, which act to generate the seed island, the amplitude fails to grow. After the ECCD is turned off, the mode amplitude stays small, as expected, until the next sawtooth crash. At that time, the amplitude increases, but it does not quite reach the 4 G level at which positive growth occurs. When the NTM is stabilized, the plasma pressure increases by an amount double that expected from the additional power represented by the ECH.

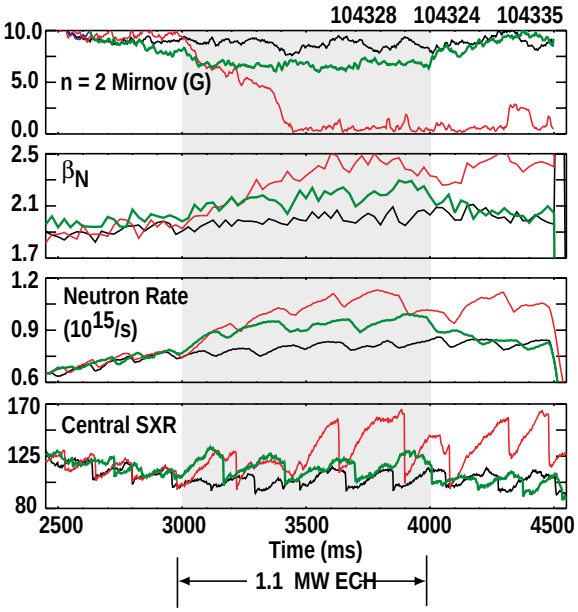


*FIG. 4. Traces from three discharges, one with ECCD applied at the q=3/2 surface (red) near ρ=0.6 and one with the ECCD moved 2 cm away from that surface (green), and one with no ECH (black)but otherwise identical. (a) amplitude of the n=2 Mirnov signal, (b) normalized beta, (c) neutron rate, and (d) central X–ray emissivity showing sawteeth. 1.1 MW of co-ECCD is applied during the shaded time. Here, $n_e(\rho=0.6)=3.9\times10^{19}$ $m^{-3}$, $T_e(\rho=0.6)=1.9$ keV, $B_T=1.5$ T, $I_p=1.2$ MA, $P_{NBI}=6$ MW.*

The stabilizing effect of ECCD shown in Fig. 4 is effective only when the location of the ECCD is very near the rational surface. This effect can be clearly seen from discharges similar to that of Fig. 4 in which the toroidal field is ramped down, thereby sweeping the location of the current deposition across the plasma. Fig. 5 shows such a case with the $B_T$ ramp starting at 2950 ms for a discharge with co-ECCD. The n=2 Mirnov amplitude decreases only when the ECCD location is sufficiently near the q=3/2 surface. (It should be noted that the island decay rate shown in Fig. 4 is smaller than the rate of change of $B_T$ shown in Fig. 5(a), so time for full stabilization is not available in this approach.) Counter-ECCD has very little effect on the mode amplitude.

The location, width, and amplitude of the calculated profile of driven current are consistent with the theoretical requirements of the stabilization process. Calculations of the driven current from the TORAY-GA code are shown in Fig. 5(c) for three different times during the

$B_T$ decay. For the early and late times the effect of the ECCD on the mode amplitude is small, while for the central time the effect is maximum, consistent with theory which says the ECCD has maximum effectiveness when placed at the center of the island. The width of the calculated ECCD profile is somewhat less than the island width as determined from ECE measurements just before the start of the $B_T$ ramp, as required for full stabilization by a continuously applied current [17]. The amplitude of the driven current density modestly exceeds the local bootstrap current density, also as anticipated by theory [17].

Figure 5 provides indirect evidence that the ECCD which is driven far off axis is close to the calculated ECCD, even in the presence of sawteeth, ELMs, and a tearing mode. If the amplitude were smaller by a factor 2 the driven current would be too much smaller than the bootstrap current to have much effect on the instability. If the profile width were much greater than the calculated profile, then the location of the driven current could not be as sensitive as that shown in Fig. 5. Hence, the NTM stabilization results imply that the ECCD obtained in the experiment is not much different than that calculated by conventional ray tracing. Detailed modeling should refine these conditions.

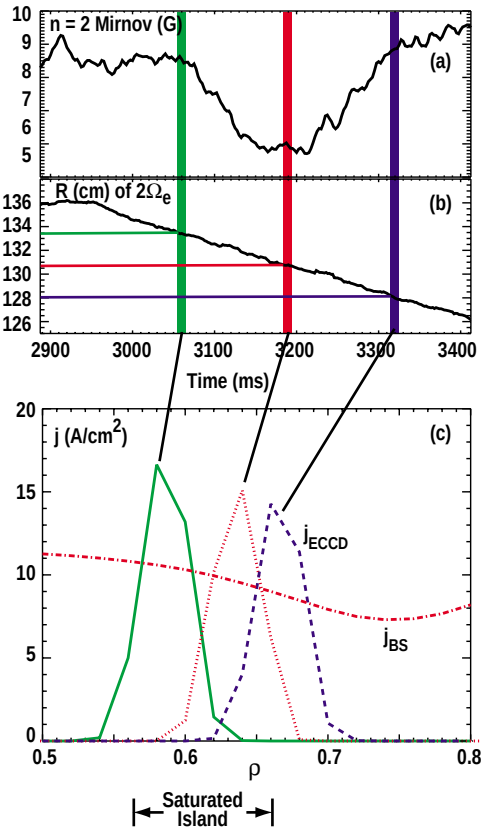


*FIG. 5. (a) Mirnov amplitude, (b) Major radius of the second harmonic of the cyclotron frequency during a scan of the toroidal field, (c) calculated ECCD for times corresponding to the arrows, for a discharge with parameters similar to those of Fig. 4.*

## 5. Improved Core Transport

Heating by ECH in the plasma core during the reversed magnetic shear conditions early in a discharge leads reliably to high electron temperatures and very large radial gradients in $T_e$. The heat diffusivity within the electron channel is much lower than ion neoclassical diffusivity in a narrow region of radius, constituting an electron internal transport barrier (eITB). Figure 6 shows traces for such a case in which counter-ECCD at a modest power of 0.5 MW was applied starting at 100 ms into the current ramp. Bursts of counter-current NBI power averaging 0.5 MW are applied for diagnostic purposes. The central electron temperature rises to 6 keV, compared to 1.2 keV for an equal amount of NBI power. Calculations of beam deposition show that little of the counter-NBI power is confined at the low plasma current, and the ion temperature stays near 0.5 keV. The effect of the neutral beam bursts is to increase $T_e$ at the shoulder of the profile, but the central heating is small. Periodic relaxations, believed to be resistive interchange modes, occur when the $T_e$ gradient becomes too large. This observation of an eITB due to electron heating by ECH during conditions of reversed magnetic shear is reminiscent of observations on FTU [18], RTP [19], ASDEX-U [20], and TCV [21].

The $T_e$ profiles shown in Fig. 7 show that the steep gradient forms just outside the heating radius. The peak of the heating moves radially outward due to the Doppler shift which grows as the electron temperature rises. The peak of the profile is flat, but the electron temperature profile develops a gradient exceeding 1.5 keV/cm just outside the heating location. Transport analysis shows that the electron diffusivity at $\rho$=0.35 is below 0.1 $m^2$/s, ten times smaller than

ion neoclassical diffusivity. The ion diffusivity also lies below neoclassical values but the ion heating is weak and the uncertainty in the diffusivity is large.

Measurements of density fluctuations in the core made by reflectometry show a reduced level in a discharge similar to that of Fig. 6, but calculations of E×B shear show that flow shear is inadequate to stabilize the low k ion temperature gradient and/or trapped electron modes, although it may reduce their net growth rates significantly. However, the electron temperature gradient mode should be only weakly affected by the flow shear. This mode may be stabilized by the combined effects of negative magnetic shear [22] and Shafranov shift [23]. Simulations using the GLF23 code, which includes the effects of the ITG, TEM, and ETG modes, predict the eITB which develops in the experiment.

Recent experiments have shown that the eITB which forms is independent of the current driven by ECCD. Comparisons of co-ECCD, counter-ECCD, and ECH without current drive show similar effects. Also, NBI power plays little role, with strongly peaked $T_e$ profiles reaching 15 keV achieved in discharges with 0.7 MW ECH and no NBI, at density near $0.7\times10^{19}$ m$^{-3}$. These results show that generation of an eITB by electron heating is a robust phenomenon.

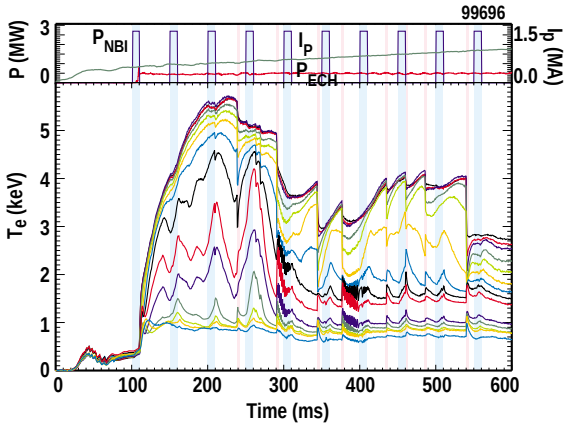


*FIG. 6. (a) Plasma current, neutral beam power, and ECH power, and (b) electron temperature from ECE for channels spaced about 2 cm in major radius. The cyan vertical stripes highlight periods of NBI and the magenta stripes identify the reconnection events. The plasma density is $0.85\times10^{19}$ m$^{-3}$.*

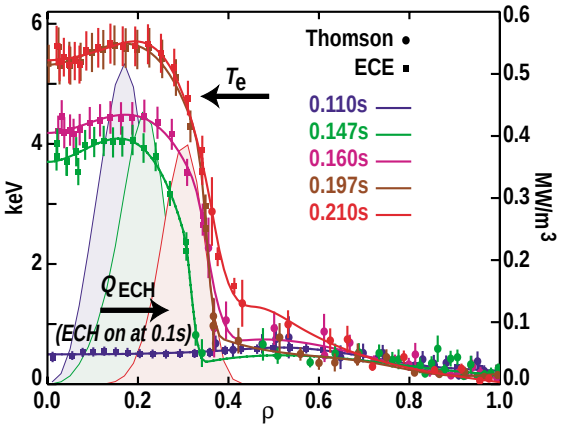


*FIG. 7. $T_e$ profiles and calculated heating profiles for different times in the discharge of Fig. 6.*

## 6. Summary

In summary, improved analysis of ECCD in quiescent L–mode discharges has shown good agreement with theory, both in magnitude and profile of the driven current. The experiments have been extended to more realistic discharges with higher performance by applying ECCD to ELMing H–mode plasmas, and the MSE data in these discharges clearly show the highly localized current drive effect. Application of ECCD to discharges with 3/2 neoclassical tearing modes results in full stabilization of the mode in good agreement with the theory of neoclassical tearing modes, a result which also supports the validity of the calculations of ECCD even under conditions of large MHD activity. The highly localized heating due to ECH can also generate an internal transport barrier for the electron component of discharges with strong negative magnetic shear. These results generally support the modeling behind the use of ECH and ECCD in providing profile control in high performance AT plasmas.


## Acknowledgment

Work supported by U.S. Department of Energy under Contracts DE-AC03-99ER54463, W-7405-ENG-48, DE-AC02-76CH03073, and Grant DE-FG05-88ER53266.

## References


[1] LUCE, T.C., *et al*., Phys. Rev. Lett. **83** (1999) 4550.
[2] LUCE, T.C., *et al*., Plasma Phys. Control. Fusion **41** (1999) B119.
[3] TURNBULL, A.D., *et al.*, Phys. Rev. Lett. **74** (1995) 718.
[4] HEGNA, C.C., and CALLEN, J.D., Phys. Plasmas **4** (1997) 2940; ZOHM, H., Phys. Plasmas **4** (1997) 3433.
[5] ZOHM, H., *et al.*, Nucl. Fusion **39** (1997) 577.
[6] CARY, W.P., *et al*., "Performance of the 1 MW 110 GHz 10 s Gyrotrons Recently Installed in the DIII–D ECH System," Proc. 21st Symp. on Fusion Tech., Madrid, Spain, (2000).
[7] PETTY, C.C., *et al*., in Radio Frequency Power in Plasmas, 13th Topical Conference, Annapolis, MD 1999, 245; in Strong Microwaves in Plasmas (Proc. 4th Int. Conf., Nizhny Novgorod, Russia, 1999) Vol. 1 (2000) 41.
[8] RICE, B.W., *et al*., Phys. Rev. Lett. **79** (1997) 2694.
[9] FOREST, C.B., *et al.*, Phys. Rev. Lett. **73** (1994) 2444.
[10] PETTY, C.C., *et al.*, "Localized Measurements of Electron Cyclotron Current Drive Using MSE Spectroscopy on the DIII–D Tokamak," General Atomics Report GA-A23388 (2000), submitted to Nucl. Fusion.
[11] LAO, L.L., *et al*., Bull. Am. Phys. Soc. **45**, DPP Annual Meeting (2000), paper NP1.079.
[12] HARVEY, R.W., and McCOY, M.C., in Proc. of IAEA Tech. Comm. Meeting, Montreal, 1992 (IAEA, Vienna, 1993) 498.
[13] SAUTER, O., *et al.*, Phys. Plasmas **4** (1997) 1654.
[14] PLETZER, A., and PERKINS, F.W., Phys. Plasmas **4** (1999) 1589.
[15] GANTENBEIN, G., *et al*., Phys. Rev. Lett. **85** (2000) 1242.
[16] A. ISAYAMA, this meeting.
[17] PERKINS, F.W., Bull Am. Phys. Soc. **45**, DPP Annual Meeting (2000), Paper NP1.092.
[18] CIRANT, S., *et al*., in Radio Frequency Power in Plasmas, 13th Topical Conference, Annapolis, MD 1999, 221.
[19] deBAAR, M.R., *et al.*, Phys. Rev. Lett. **78** (1997) 4573.
[20] WOLF, R.C., *et al*., Phys. Plasmas **7** (2000) 1839.
[21] PIETRZYK, Z.A., et al., in 27th EPS Conf. on Control. Fusion and Plasma Physics, Budapest (2000), Paper P4.099.
[22] WALTZ, R. *et al.*, Phys. Plasmas **4** (1997) 2482.
[23] DOYLE, E.J., *et al.*, this meeting.